2nd Draft (06/14/07), Submitting to *Bull. Seismol. Soc. Am.,*

Crustal Velocity Structure in Italy from Analysis of Regional Seismic Waveforms

Hongyi Li, [1] Alberto Michelini, [1] Lupei Zhu, [2] Fabrizio Bernardi, [1] and Matteo Spada[3]

Istituto Nazionale di Geofisica e Vulcanologia, Via di Vigna Murata, 605, Rome 00143, Italy. (email:hongyili@ingv.it)

Abstract. In this paper, we use regional seismic waveforms recorded by the recently-installed Istituto Nazionale di Geofisica e Vulcanologia (INGV) national network and the Mediterranean Very Broadband Seismographic Network (MedNet) stations to develop one-dimensional (1-D) crustal velocity models for the Italian peninsula. About 55,000 P-wave and 35,000 S-wave arrival times from 4,727 events are used to derive average seismic parameters in the crust and uppermost mantle. We define four regions, according to geological constraints and recent travel-time tomography results. Based on the average seismic parameters, we combine broadband seismic waveforms and travel-times of regional phases to model crustal structures for the four regions by applying the genetic algorithm. Our results indicate smooth velocity gradients with depth beneath the Apennines, and a deep Moho beneath the central Alps. Green's functions from the regionalized 1-D velocity models are used to determine source depths and focal mechanisms for 37 events with magnitude larger than 3.5 by a grid search technique. Our results show that normal and strike-slip faulting source mechanisms dominate the Apenninic belt and most thrust faulting events occur in the Adriatic sea and the outer margin of the northern Apennines.

Introduction

Knowledge of the velocity structure of a region is a fundamental ingredient toward calculation of Green's functions. The final and long term goal being, for each region, the compilation of a database of readily accessible Green's functions to be used after an earthquake for the rapid and automatic modeling of the full seismic wavefield at frequencies of engineering interest. The main purpose of this study is to define reference velocity models for the Italian peninsula from regional seismic waveform analysis. The Green's functions obtained using these models can be used effectively for generating more accurate near-real-time extended fault inversion and, in the future, maps of the ground shaking.

A well defined velocity structure is also important for source mechanism determination. Although local propagation effects can be particularly relevant at short periods, signals in the period range of 2–10 s are thought to remain stable over local geological provinces [*Zhu et al.*, 2006]. Thus, Green's functions for local 1-D velocity model can be used successfully in many places.

Most of information on the the crustal structure of Italy comes from travel-time tomography studies [e.g. *Alessandrini et al.*, 1995; *Chiarabba and Amato*, 1996; *Chiarabba and Frepoli*, 1997; *Di Stefano et al.*, 1999]. However, the travel-time inversion technique generally suffers from relevant velocity-depth trade-offs resulting in model non-uniqueness. On the other hand, the

[1]Istituto Nazionale di Geofisica e Vulcanologia, Via di Vigna Murata, 605, Rome 00143, Italy

[2]Department of Earth and Atmospheric Sciences, Saint Louis University, St Louis, USA

[3]Institute of Geophysics, ETH-Honggerberg, CH-8093 Zurich, Switzerland

waveform inversion method can reduce velocity-depth trade-offs, since whole waveforms contain more information about crustal structure than narrowly selected parts of seismograms such as arrival times [*Dreger and Helmberger*, 1990; *Rodgers and Schwartz*, 1998; *Du and Panza*, 1999]. In this work, in order to reduce the velocity-depth trade-off, we use a joint inversion of regional seismic waveforms and travel-times to derive the best 1-D velocity models for different regions by applying the genetic algorithm (GA) [e.g. *Holland*, 1975; *Goldberg*, 1989]. The regionalization is based on geological constraints and recent tomography results from high-quality *P*-wave arrival times [*Di Stefano et al.*, 2006]. Green's functions from these 1-D velocity models are used to retrieve the source parameters for events with magnitude larger than 3.5 using the modified Cut-and-Paste (CAP) method [*Zhu and Helmberger*, 1996].

Tectonic Setting and Previous Results

The geodynamic evolution of Italy is controlled by the relative motion between the Eurasian and African plates since at least 65 Ma ago [*Malinverno and Ryan*, 1986; *Dewey et al.*, 1989; *Patacca et al.*, 1990]. The N-S convergence between these two continental plates resulted in a fragmentation of the lithosphere into several microplates [*Westaway*, 1990; *Gvirtzman and Nur*, 2001; *Margheriti et al.*, 2003]. The complex interaction among these microplates led to a jigsaw-puzzle-like tectonics, and the present tectonic structure of Italy is dominated by the formation of the Alps, the orogenesis of the Apennines and the opening of the Tyrrhenian basin [*Patacca and Scandone*, 1989]. The Apennines consists of two major arcs (the northern Apenninic and the Calabrian Arcs) and a complex area (the central-southern Apennines) in between (Fig. 1). The complexity is probably responsible for the lateral heterogeneities in the lithospheric structure.

The crustal structure of Italy has been investigated by applying different seismic methods. From inversion of *P*-wave travel-time, *Chiarabba and Frepoli* [1997] obtained 1-D velocity models for central and southern Italy. Their results indicated that there is no obvious velocity discontinuity for central and southern Italy, the *P*-wave velocity in the upper crust is between 5.2 km/s and 5.9 km/s, in the lower crust between 6.2 km/s and 6.8 km/s. However, they assumed the Moho depth (35 km) and the thickness of each layer are the same for central and southern Italy in their 1-D models. By inverting a large amount of *P*-wave arrival times, *Alessandrini et al.* [1995],*Chiarabba and Amato*

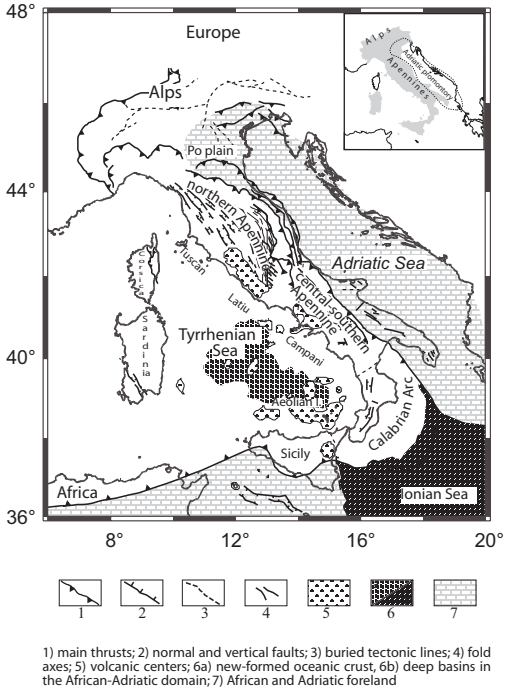

Figure 1. Tectonic sketch of the Italian region, from *Margheriti et al.* [2003].

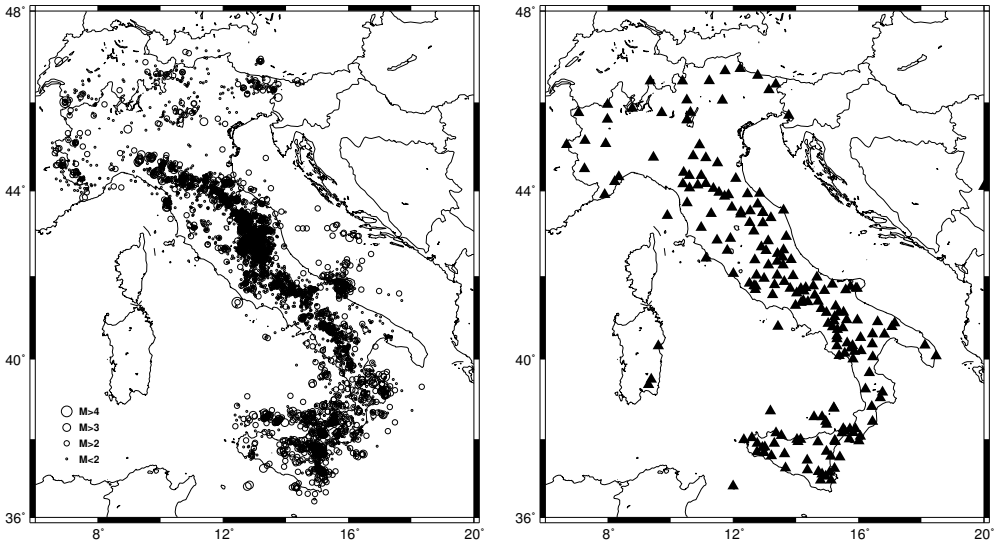

Figure 2. Left: Distribution of events(circle) used for travel-time fitting; Right: Seismic stations(triangle) used in this study.

[1996],*Di Stefano et al.* [1999], *Paul et al.* [2001],and *Di Stefano et al.* [2006] calculated three-dimensional crustal velocity structures of Italy. *Mele and Sandvol* [2003] and *Amato et al.* [1998] estimated the Moho depth beneath the northern Apennines and central Italy by studying teleseismic receiver functions recorded by a regional array. By measuring group velocities of surface waves, *Pontevivo and Panza* [2002] derived average S-wave velocity structures of the crust and upper mantle for different regions in Italy. The average model of the Apennines belt from their results showed that the Moho depth in this region is about 40 km, and a low-velocity layer with S-wave velocity around 2.5 km/s is located at 10 to 15 km in contrast with some previous results [*Chiarabba and Frepoli*, 1997; *Amato et al.*, 1998]. There were also several deep seismic refraction profiles from Corsica to the Italian Adriatic coast [*Scarascia et al.*, 1994; *Ponziani et al.*, 1995; *Hirn and Sapin*, 1997], in the northern sector of the Southern Apennines belt [*Improta et al.*, 2000], and reflection surveys across the northern Apennines [*Barchi et al.*, 1998; *Gualtieri and Cassinis*, 1998; *Gualtieri et al.*, 1998]. Upper mantle structure beneath Italy has been studied by *Amato et al.* [1993], *Spakman et al.* [1993], *Selvaggi and Chiarabba* [1995], *Piromallo and Morelli* [1997], *Amato et al.* [1998], *Mele et al.* [1998], *Di Stefano et al.* [1999], and *Piromallo and Morelli* [2003]. In general, results from these studies show that the average Moho depth for the Apenninic belt is about 34–38 km. The average P velocity in the crust is around 6.2 km/s and Pn in the uppermost mantle between 7.4 km/s and 8.0 km/s. Lateral heterogeneities are reported in many studies. For example, P-wave travel-time tomography studies [*Chiarabba and Amato*, 1996; *Chiarabba and Frepoli*, 1997] revealed that on the Adriatic side of the Apennines the Moho tends to be deeper than 37 km and on the Tyrrhenian side the Moho depth is between 22 and 34 km.

Velocity structure from arrival time analysis

In this study, we first use about 55,000 P-wave and 35,000 S-wave arrival times from 4,727 events occurred in Italy and surrounding regions between January 2005 and November 2006 (Fig. 2), to compute average seismic parameters in the crust and uppermost mantle. Because we focus more on the crustal structure, hypocentral depths of selected events are confined to be less than 40 km. Fig. 3 shows travel-times versus epicentral distances for the first P and S arrivals. The arrival times have weights of 0 to 4 assigned depending on quality of pick, 0 represents the best and 4 represents the least reliable. The average P-wave velocity in the crust estimated from Fig. 3 is 6.21 km/s and S-wave velocity is 3.48 km/s, which agree with previous studies [*Chiarabba and Amato*, 1996; *Chiarabba and Frepoli*, 1997; *Pontevivo and Panza*, 2002]. Since there are few

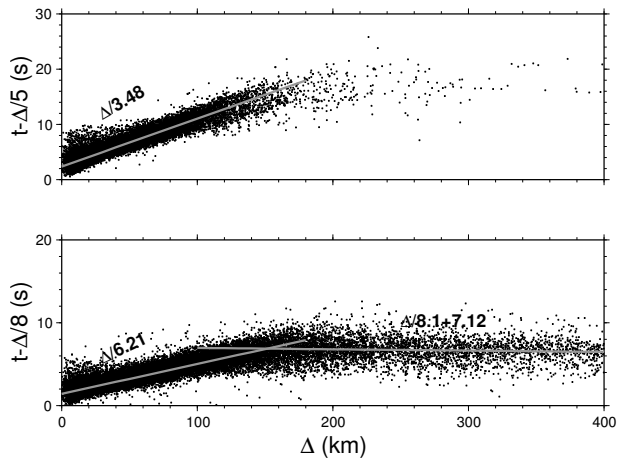

Figure 3. Travel-times versus epicentral distances of first P (bottom) and S (top) arrivals. Travel-times are reduced with $Vp = 8\ km/s$ and $Vs = 5\ km/s$.

S arrivals beyond epicentral distance of 160 km, we only estimate Pn velocity (8.1 km/s) in the uppermost mantle. By assuming a shallow source depth of 12 km, the crustal thickness estimated from the Pn intercept time is about 34 km, which is consistent with the average Moho depth beneath the Apenninic belt from teleseismic receiver function studies [*Amato et al.*, 1998].

1-D velocity models from GA inversion

Since the shallow crustal structure has a strong effect on regional surface waveforms [e.g. *Song et al.*, 1996], the seismic parameters in the crust estimated from arrival time data is further fine-tuned by waveform inversion with the genetic algorithm.

Method

The GA is a robust and efficient direct global search method for solving nonlinear problems with many local minima. The GA begins with many initial models, which are randomly generated within prescribed ranges of model parameters. Then through a selection process which privileges higher fitness values to be selected, the GA proceeds by repeated application of genetic operators such as mutation and crossover to evolve the solutions in order to find the best model. The crossover operator generates new pairs of models by an exchange of some information between paired models. The mutation operator introduces a certain amount of randomness to the search by allowing model parameters to jump arbitrarily to other points in the model space, therefore it can help the search to find solutions that crossover alone might not encounter. As a result, different from the iterative linearized approach in which the final solution depends intrinsically on the starting model, the GA attempts to find an optimal solution by considering all of the regions of the defined search space. The GA has been applied to many geophysical problems such as velocity structure estimation [*Zhou et al.*, 1995; *Bhattacharyya et al.*, 1999; *Louis et al.*, 1999; *Chang et al.*, 2004; *Chang eand Bagg*, 2006], source parameters and site effects [*Kobayashi and Nakanishi*, 1994; *Moya et al.*, 2000], seismic source rupture process [*Zeng and Anderson*, 1996] and hypocenter location [*Kennett and Sambridge*, 1992; *Billings et al.*, 1994; *Kim et al.*, 2006].

The fitness function that we have adopted for the GA is defined as follows:

$$F_k = (1 - w_1 - w_2)\frac{\sum_i cc_i}{N_w} - w1\frac{\sqrt{\sum_i \sum_j (O_{ij} - S_{ij})^2}}{N_w \sqrt{\sum_i \sum_j O_{ij}^2}} - w_2 \frac{\sqrt{\sum_j (t_j^{obs} - t_j^{cal})^2}}{N_t}, \quad (1)$$

where F_k is the fitness value of the kth velocity model, cc_i is the cross-correlation coefficient between the ith observed data and synthetic seismogram, N_w is the number of observed data. O_{ij} is the amplitude of observed data at the jth sampling time of the ith component, S_{ij} is the synthetic seismogram amplitude at the jth sampling time of the ith component, t_j^{obs} and t_j^{cal} are the jth observed and calculated travel-time, respectively, N_t is the number of travel-time data, and w_1, w_2 are the weight parameters that balance the misfits of waveform data and travel-time data. In equation (1), the first term measures waveform similarity between observed data and synthetics, the second term represents the misfit of waveform amplitude, and the third term measures the travel-time difference.

We first test the robustness of the GA inversion. In the numerical test, the source depth is 18 km, the station is 184.4 km away from the epicenter. Synthetic seismograms from the true velocity model, which is defined by the thick solid line in Fig. 4, are used as input data. Nine model parameters for a 1-D velocity model with four layers in the crust are used in our inversion: the P-wave velocity and depth of each layer and crustal Vp/Vs ratio. The Pn velocity during the inversion is fixed at 8.1 km/s. A time window of 120 s starting from the event origin time is used in the inversion. We set

the population size to 20 and run the GA inversion for 100 generations with five randomizing seed values in the test, then the final resolved velocity model is obtained by averaging the five best models. Standard deviations are also computed. The averaged model and waveforms generated from this model are shown in Fig. 4. All the waveforms are bandpass filtered between 0.02 Hz and 0.1 Hz and plotted with absolute amplitudes. The waveforms show an excellent agreement between the data and synthetics.

Data and analysis

The GA inversion is applied to estimate the crustal velocity structure in the Italian peninsula. We use regional seismic waveforms recorded at recently installed broadband stations and high quality Pg and Pn arrival times which have been reviewed by seismologists. Considering structural heterogeneities in the Italian peninsula, we only pick stations within a distance of 280 km from the epicenter. We exclude records with low signal-to-noise ratio by inspecting the seismograms. A total of 19 events with magnitude between 4.0 and 5.2, and 42 stations that cover most of the Italian peninsula are selected for the GA inversion. Locations of the events and stations are shown in Fig. 5. Event locations and source mechanisms used in the GA inversion are from the INGV bulletin (http://www.ingv.it). When the source mechanism was not listed, we determined it using the minimum 1D velocity models of *Chiarabba and Frepoli* [1997]. In our inversion, we use only the direct P-wave arrivals recorded at stations with epicentral distances smaller than 90 km, and Pn-wave arrivals with epicentral distances larger than 180 km. This choice avoids phase misidentification between the direct P and Pn.

With the recent travel-time tomography results from high quality P-wave arrival times [*Di Stefano et al.*, 2006], we compute the average P-wave velocity for the upper 22 km in the crust by averaging the P-wave velocities from the first layer (at 8 km depth) and the second layer (at 22 km depth) of *Di Stefano et al.* [2006]'s three-dimensional P-wave velocity models (Fig. 5). Then by taking into account the average P-wave velocity, geological setting and source receiver geometry, we divide the Italian peninsula into four subregions which are shown in Fig. 5. Region I can be associated with most of the central Alps; Region II with the northern Apennines; Region III with the central Apennines; Region IV with the southern Apennines and Calabria because of few events in the southern Apennines and similar average crustal P-wave velocities in the southern Apennines and Calabria. The starting 1-D velocity model has four layers in the crust by considering the information provided by previous studies. We perform the GA inversion with 100 generations for five times to obtain the best-fit velocity model for each region.

A total of 8 event-station pairs from 5 events are used for the central Alps (Fig. 5). The best 1-D velocity model (Fig. 6(I)) consists of 4 layers in the crust with a crustal thickness of 51.0±2.0 km. The P-wave velocities are 4.60±0.22, 5.85±0.16, 6.10±0.18 and 6.30±0.20 km/sec from the top layer to the forth layer, respectively, the depths of layers are 2.2±0.9, 9.0±1.1, 25.0±1.8 and 51.0±2.0 km, and the Vp/Vs ratio is 1.79±0.04. The Moho depth of 51.0±2.0 km is consistent with earlier studies from wide-angle seismic studies [*Scarascia and Cassinis*, 1997; *Waldhauser et al.*, 1998, 2002] and teleseismic receiver function analysis [*Kummerow et al.*, 2004]. The low velocities in the upper crust may indicate thick sedimentary deposits in this region. The synthetic waveforms generated from the above 1-D model are compared with the observed waveforms in Fig. 7. These are velocity waveforms bandpass filtered between 0.02 Hz and 0.1 Hz. Since the Alpine region is tectonically quite complex, waveform fits from our 1-D model still show obvious differences between synthetics and observations. The differences are interpreted as being caused by lateral variations of velocity structure that can not be accounted in the 1-D layered velocity model. Meanwhile, we also compare our best-fit 1-D model with the velocity model we averaged from *Di Stefano et al.* [2006]'s three-dimensional P-wave velocity model with a fixed Moho depth of 35 km (Fig. 7). Generally, the 1-D velocity model obtained from this study produces somewhat better fits of the waveforms and the travel-times than those from the averaged model from tomography.

A total of 29 event-station pairs from selected 4 events are used in the northern Apennines (Fig. 5). The best 1-D velocity model (Fig. 6(II)) for the northern Apennines has a crustal thickness of 35.2±1.2 km. The P-wave velocities are 5.03±0.12, 5.88±0.10, 6.01±0.10 and 6.64±0.07 km/sec from the top layer to the forth layer, respectively, the depths of layers are 7.2±0.5, 12.0±1.0, 23.0±1.2 and 35.2±1.2 km, and the Vp/Vs ratio is 1.84±0.02. We compare the synthetics generated from the best 1-D velocity model with the model averaged from the tomographic model of *Di Stefano et al.* [2006], and also the minimum 1-D velocity model from *Chiarabba and Frepoli* [1997]. As shown in Fig. 8 at station ARCI and SACS, it is clear that the synthetics computed from the two models are earlier than the

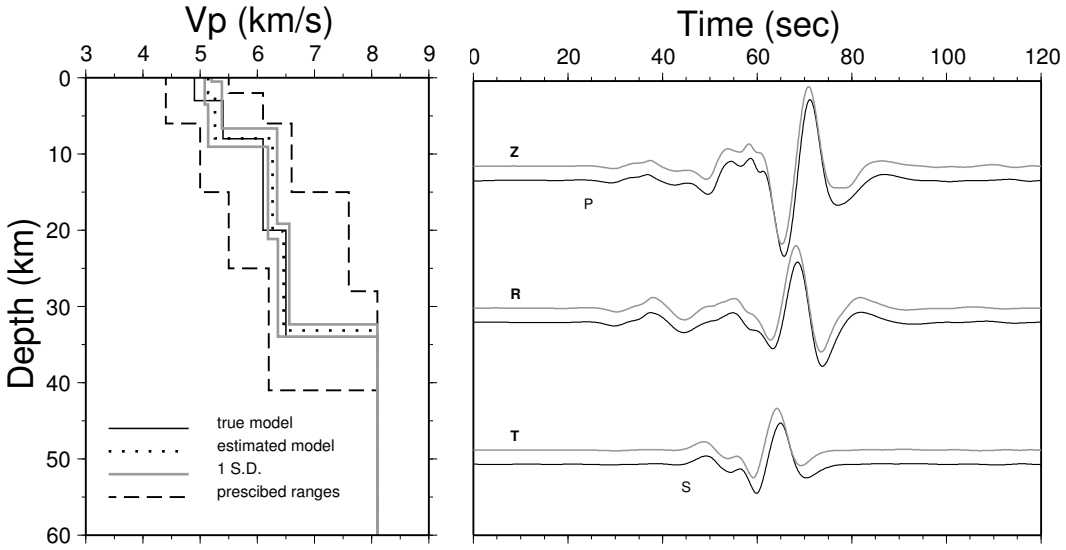

Figure 4. Left: A comparison of the estimated average velocity model with the true model in the numerical test. Thick solid line indicates the true model, the dotted line is the estimated average velocity model, thin solid lines represent ±1 standard deviation for each model parameter, and dashed lines denote the prescribed lower and upper limits of velocity and depth range in which the model parameters are allowed to be changed in the inversion. Right: A comparison of three-component waveforms generated from the estimated average velocity model (gray) with the input waveforms (black).

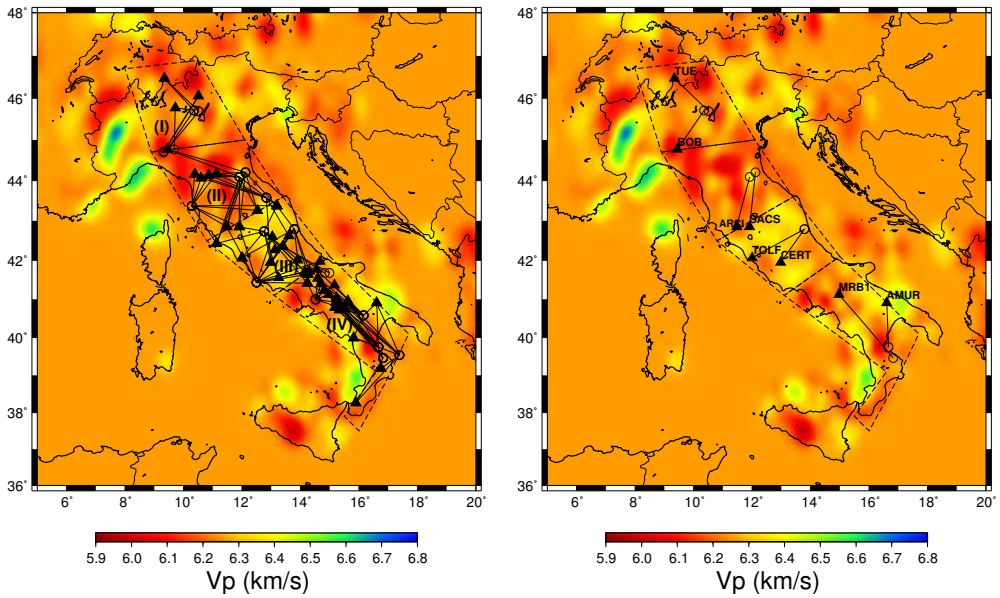

Figure 5. Left: map of events (circle) and stations (triangle) used for the GA inversion. The four sub-regions are based on recent P-wave travel-time tomography results from *Di Stefano et al.* [2006]. The average P-wave velocities for the upper 22 km in the crust are shown. (I) central Alps; (II) northern Apennines; (III) central Apennines; (IV) southern Apennines. Right: map of event-station pairs used for waveform comparison between the best velocity models from this study with other models.

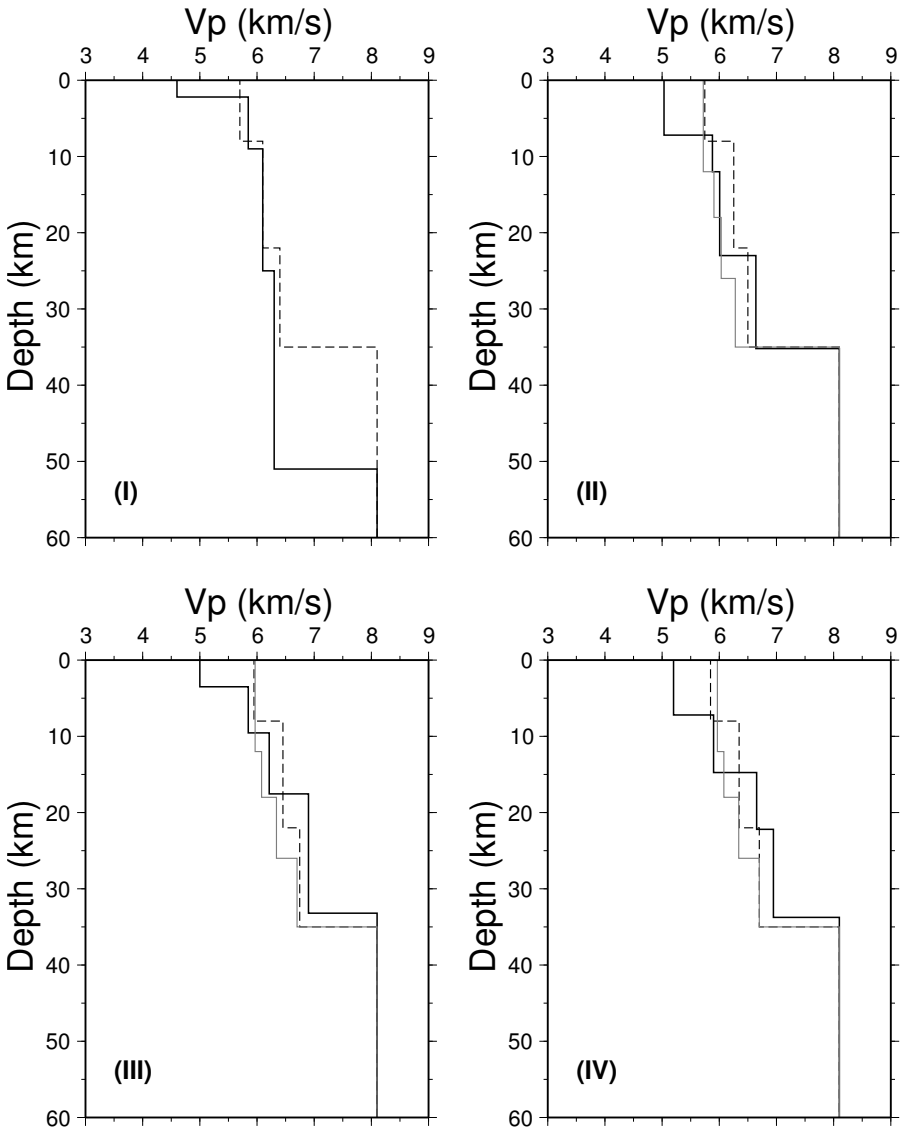

Figure 6. Comparison of velocity models from this study (solid line) with the velocity models averaged from recent *P*-wave tomography results (dashed line), and the minimum 1D velocity models from *Chiarabba and Frepoli* [1997] (gray line, they do not include the central Alps region) for the four subregions. (I) central Alps; (II) northern Apennines; (III) central Apennines; (IV) southern Apennines.

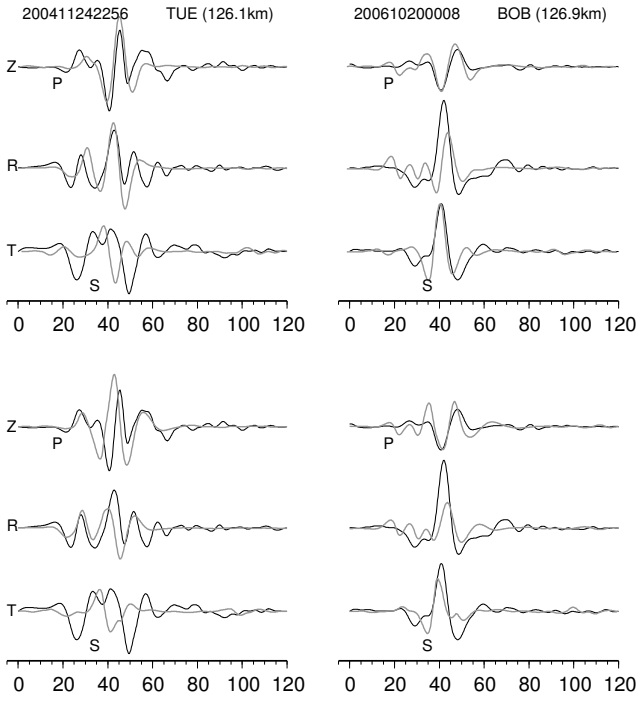

Figure 7. Comparison of synthetic waveforms with observation for Region (I), the central Alps. Top: Comparison of synthetic waveforms from the best-fit velocity model obtained in this study (gray) with observed waveforms (black). Bottom: Comparison of synthetic waveforms from the velocity model averaged from recent P-wave tomography results (gray) with observed waveforms (black). Time is relative to the event's origin time. P- and S-wave arrivals are estimated from the best-fit velocity model.

observed data, and that the synthetics generated from the velocity model determined in our study provide a better fit.

A total of 36 event-station pairs from 5 events are used for the GA inversion in the central Apennines (Fig. 5). The Moho depth in the central Apennines from the GA inversion (Fig. 6(III)) is at 33.2±1.8 km. From the surface layer to the forth layer, the P-wave velocities are 5.00±0.15, 5.85±0.10, 6.21±0.12 and 6.90±0.15 km/sec, respectively. The depths of the four layers are 3.5±1.0, 9.6±0.4, 17.6±0.5 and 33.2±1.6 km, and the Vp/Vs ratio is 1.83±0.03. In general, synthetics from our velocity model fit the observed data well on waveform shape, amplitude and arrival time except for the transverse component at station TOLF (Fig. 9). At station TOLF for this earthquake the SH-wave has small amplitude because it is close to the node of SH-wave radiation pattern. This may result in the difficulty for waveform fitting at station TOLF.

A total of 43 event-station pairs from 5 events are selected for the GA inversion in the southern Apennines (Fig. 5). The best 1-D velocity model for the southern Apennines from the GA inversion is presented in Fig. 6(IV). The P-wave velocities in the model are 5.20±0.20, 5.90±0.11, 6.65±0.15, and 6.95±0.18 km/sec from the top layer to the forth layer, the depths are 7.2±1.5, 14.7±1.5, 22.2±1.2, and 33.7±1.7 km. The waveforms from the best 1-D model are compared with the observed waveforms in Fig. 10. The waveform fitting in the southern Apennines is not as good as in the northern and central Apennines due to the inclusion of different tectonic units. However, the 1-D velocity model derived from the GA inversion still produces better fits of the waveforms and the travel-time data than the other two models (Fig. 10).

In Fig. 11 we compare the fitness values for the total 116 event-pairs for the velocity models derived from our study with those obtained from tomography. By combining waveform and travel-time data in the GA inversion, our velocity models show generally higher fitness values than those obtained from the other models. Fig. 12 gives the average fitness values for 19 events and 42 stations. Overall, the northern and central Apennines show relatively high fitness values. In the southern Apennines, however, the fitness values are lower because of the large lateral variations shown in Fig. 5. We also notice that events occurred on the Adriatic side of the Apennines have larger fitness values than those on the Tyrrhenian side. This suggests that our models are more appropriate for the Adriatic side of the Apennines. This interpretation is consistent with the previous stud-

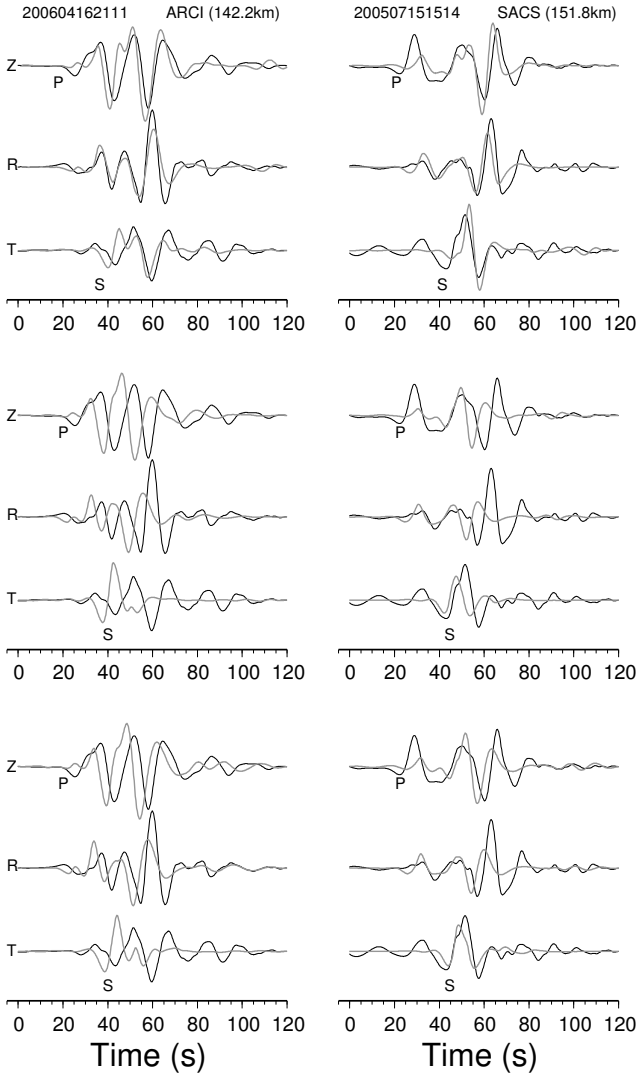

Figure 8. Comparison of synthetic waveforms with observation for Region (II), the northern Apennines. Top: Comparison of synthetic waveforms from the best-fit velocity model obtained in this study (gray) with observed waveforms (black). Middle: Comparison of synthetic waveforms from the velocity model averaged from recent P-wave tomography results (gray) with observed waveforms (black). Bottom: Comparison of synthetic waveforms from the minimum 1D velocity model from *Chiarabba and Frepoli* [1997] (gray) with observed waveforms (black).

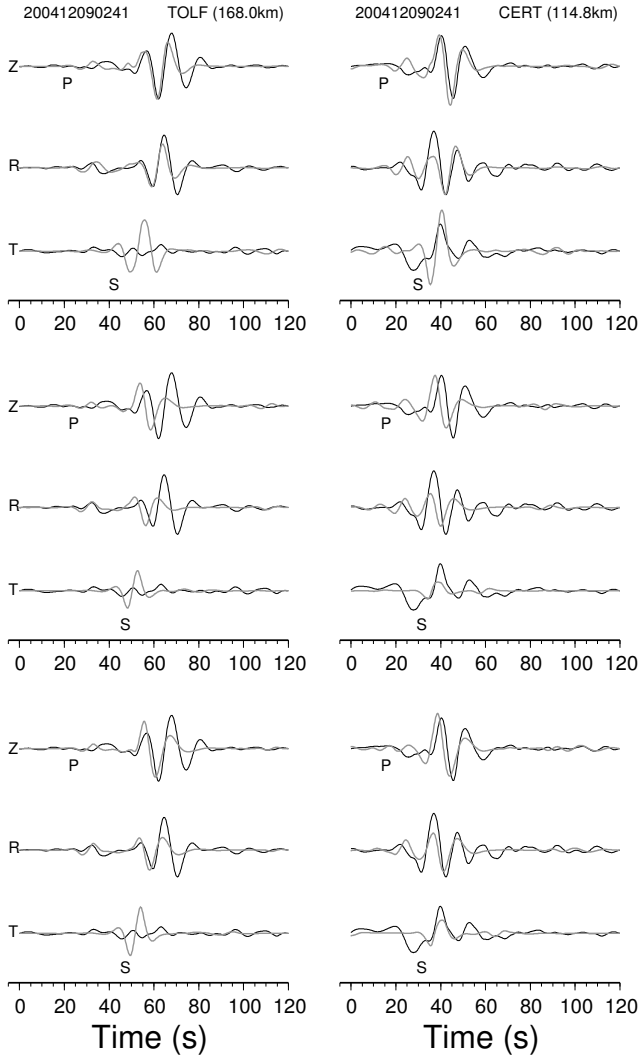

Figure 9. Comparison of synthetic waveforms with observation for Region (III), the central Apennines. All symbols and descriptions are the same as those given in Fig. 8.

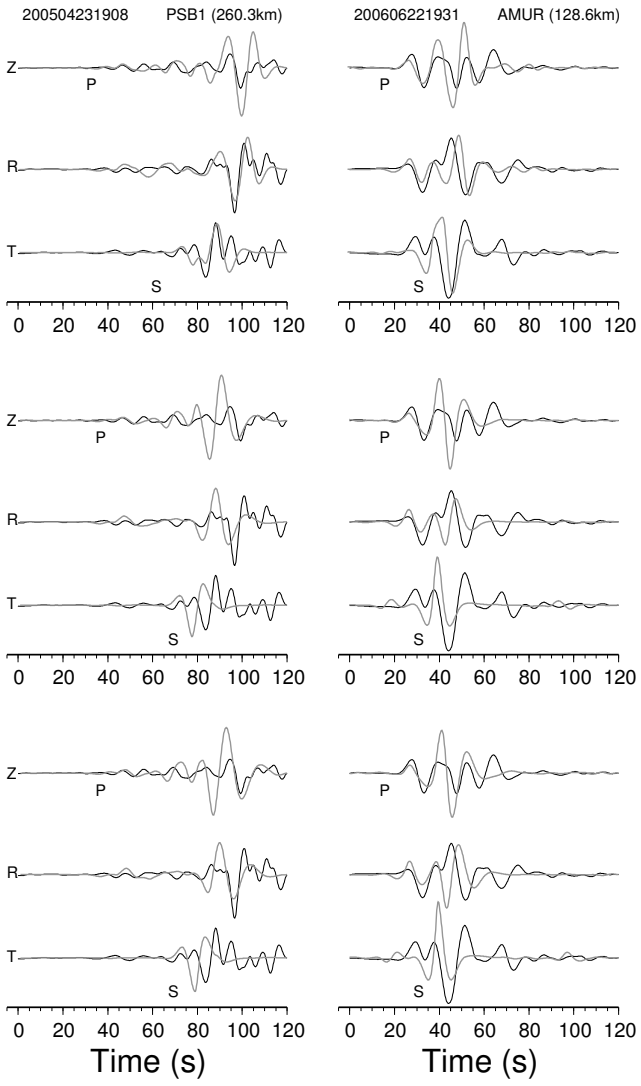

Figure 10. Comparison of synthetic waveforms with observation for Region (IV), the southern Apennines. All symbols and descriptions are the same as those given in Fig. 8.

ies [*Chiarabba and Amato*, 1996; *Chiarabba and Frepoli*, 1997; *Pontevivo and Panza*, 2002], which show a shallower Moho depth (<34 km) on the Tyrrhenian side of the northern Apennines with respect to the Adriatic side. Fig. 13 shows a comparison of the observed P-wave arrival times, the predicted first arrival times from velocity models obtained in this study and velocity models averaged from recent P-wave tomography results. It is clear that our velocity models improve significantly the fit to the arrival times. Nonetheless, there are still discrepancies between observed and predicted arrival times from the use of the resolved models. These differences are also imputable to the inversion procedure itself that attempts to fit both arrival times and waveforms simultaneously within an idealized 1D velocity structure.

Source Mechanisms Analysis

Once reliable 1-D velocity models become available, their theoretical response can be computed and source mechanisms be estimated from observed waveforms. In this study, Green's functions of the 1-D model are computed using a frequency-wavenumber (F-K) integration method [*Zhu and Rivera*, 2002] for distance ranges from 50 to 300 km on a grid of 5 km spacing and depth ranges from 3 to 50 km with a 2 km spacing. Source depths and focal mechanisms are determined through a direct grid search technique, which breaks up a whole broadband regional waveform into the *Pnl* (extended P-wave) and surface wave segments, and minimizes the misfit in the *Pnl* and surface waves separately. The method was originally proposed by *Zhao and Helmberger* [1994]. *Zhu and Helmberger* [1996] modified the method to deal with data recorded by stations near nodes of radiation pattern. One of the advantages of this method is that a certain amount of time shift is allowed between the observed and synthetic waveforms during the inversion.

We use the regionalized 1-D velocity models determined in this study to estimate source depths and focal mechanisms for 37 events in the magnitude range of 3.5–5.2. Fig. 14 shows an example of waveform fits produced by the modified CAP inversion. As seen in the figure, the seismograms are decomposed into *Pnl* and surface wave segments that are fitted separately. We bandpass filter the *Pnl* waves between 0.08 Hz and 0.4 Hz, and surface waves between 0.02 Hz and 0.1 Hz. Body waves are less affected by shallow heterogeneities and more stable than surface waves, although they have a lower signal-to-noise ratio due to their smaller energy. For

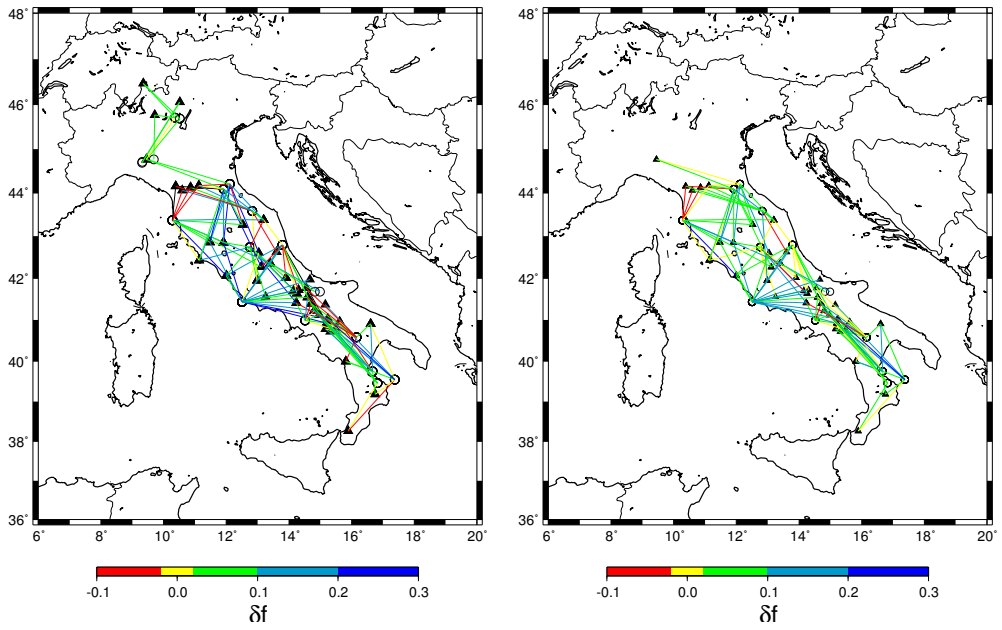

Figure 11. Left: Differences between the fitness values from our velocity models and velocity models averaged from recent P-wave tomography results. Positive indicates that fitness values from our models are higher than the models from recent P-wave tomography results, i.e., synthetics computed from our velocity models fit observations better than those from recent P-wave tomography results. Right: comparison of fitness values from our velocity models and the minimum 1D velocity models from *Chiarabba and Frepoli* [1997].

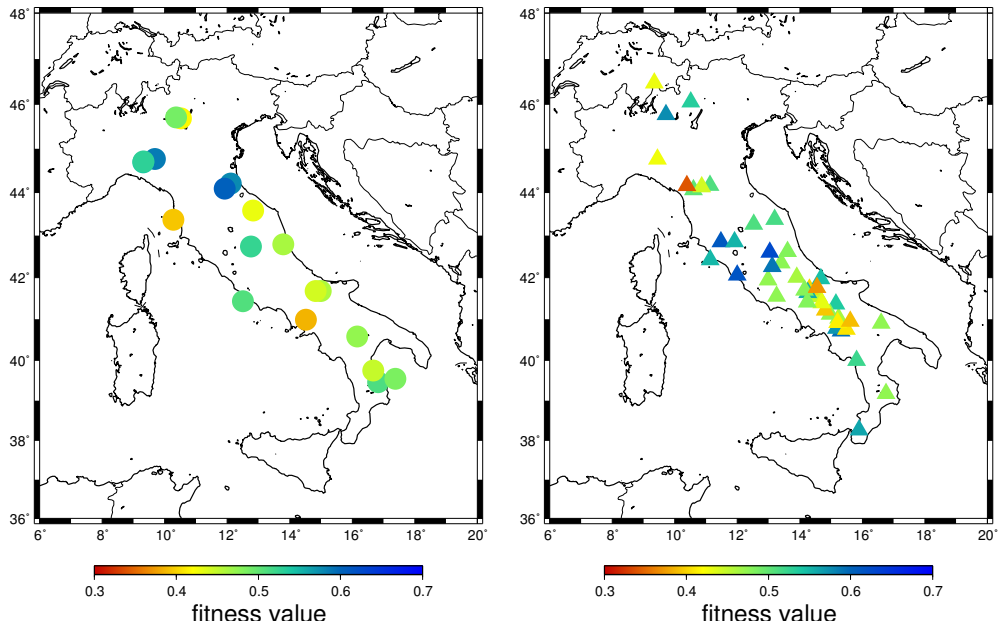

Figure 12. Fitness values calculated from the velocity models determined in this study for all events and stations used in the GA inversions. Left: fitness values for each event. Right: fitness values for each station.

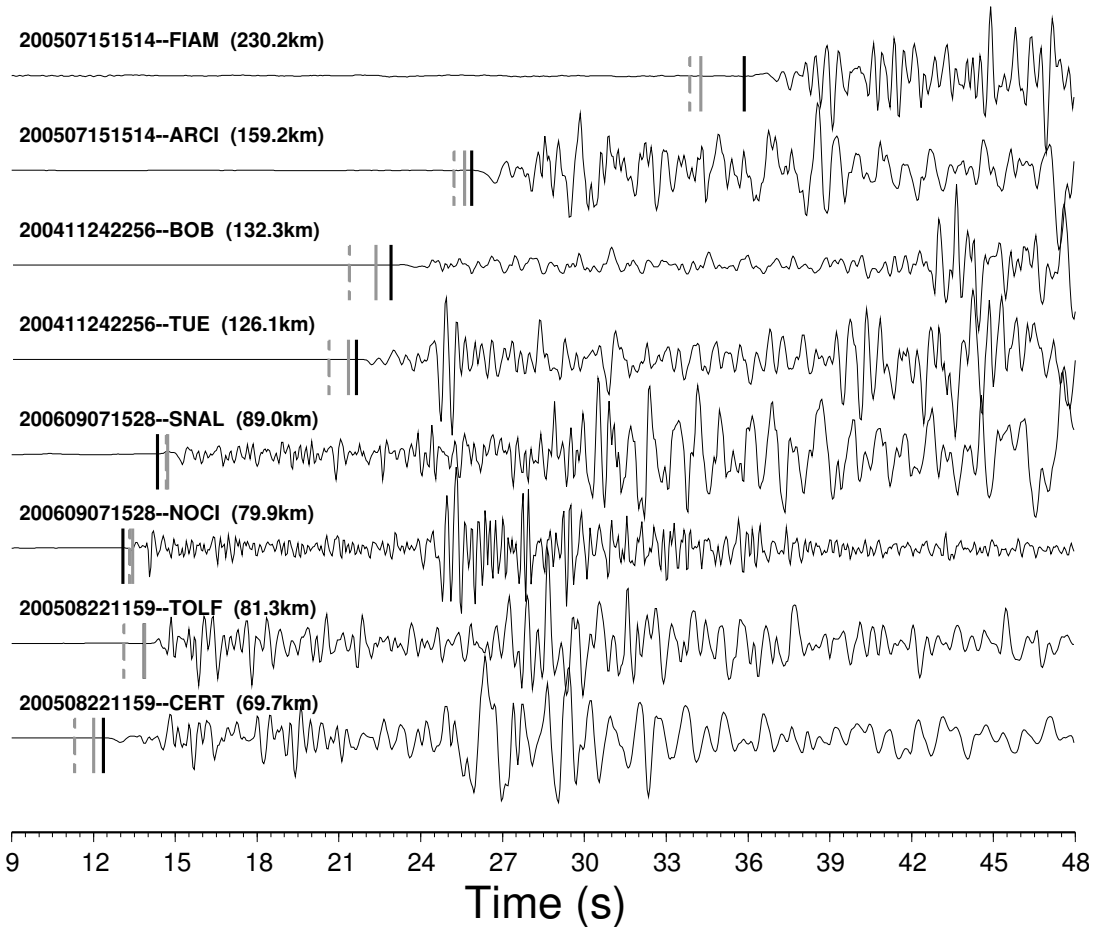

Figure 13. A comparison of the observed P-wave arrival times (black bar), and the predicted first arrival times (gray bar) based on velocity models obtained in this study, and the predicted first arrival times (dashed bar) using velocity models averaged from recent P-wave tomography results. Time is relative to the event's origin time. The event and station names plus epicentral distances are shown above the trace.

this reason, we put more weight on the body wave part relative to surface waves by multiplying the *Pnl* amplitudes by a factor of 2. The left two columns show the waveform fits for *Pnl* waves. The next three columns show the waveform fits of surface waves. The numbers below each waveform segment are the time shifts in seconds and the cross-correlation coefficients. In general, with the modified CAP method, the synthetics fit the observations well both in shape and amplitude.

In order to verify the accuracy of the method, we have first selected 8 events with $Mw \geq 4.5$ which solution had been previously determined using the Regional Centroid Moment Tensor (RCMT) method [*Ekström et al.*, 1998] from MedNet (http://mednet.rm.ingv.it/rcmt.php; *Pondrelli et al.* [2006]). As shown in Fig. 15, the results obtained using the two methodologies agree generally well. In addition to RCMT, the focal mechanism solutions presented below obtained with the CAP method have been compared to the time-domain moment tensors (TDMT) that INGV determines routinely (http://earthquake.rm.ingv.it/tdmt.php; *Scognamiglio et al.* [in preparation]) using the methodology of *Dreger and Helmberger* [1993]. In general, the results obtained with the two methods agree well with the exception of one event. In which case, the TDMT solution quality was not well constrained ("C" quality) and the difference can be attributed to the fact that CAP, because it uses higher frequency *Pnl* waves, features a larger resolving power than lower frequency methods.

The next step has been to determine the source depths and focal mechanisms for 29 events with $Mw > 3.5$ using the the regionalized velocity models above. Focal mechanisms and depths of the entire set of 37 events are listed in Table 1 and are plotted in Fig. 15. In addition and to the purpose of having a better overall perspective of the focal mechanisms throughout the Italian territory and adjacent areas, we plot in Fig. 15 also the focal mechanisms for 26 $Mw > 4.0$ events from MedNet.

Beneath the Adriatic sea and the eastern side of the northern Apennines, most events show thrust faulting in agreement with the N-S compression of this area. Normal fault events occurred mostly beneath the Apennines belt, which is consistent with the regional NE-trending extension [*Westaway*, 1992; *Montone et al.*, 1999]. Strike-slip fault events with a NE extension axis also occurred mostly beneath the Apennines which are probably related to secondary structures in the Apennines area. The distribution of source mechanisms from our determination show a good agreement with results of *Chiarabba et al.* [2005], who reviewed the focal mechanisms of large events with magnitudes larger than 4.5 in the past 20 years.

Discussion and Conclusions

In this paper, we have determined 1-D average velocity models for the Italian peninsula from the joint inversion of regional seismic waveform and travel-time data. In the central Alps, our velocity model gives a Moho depth of 51.0±2.0 km and a low P-wave velocity in the upper crust, which is consistent with previous studies [*Waldhauser et al.*, 1998, 2002; *Kummerow et al.*, 2004]. According to their studies, the European Moho dips to the south down to more than 50 km depth beneath the central Alps, and low crustal P-wave velocities are the result of thick terrigenous sediments underneath the Alps. The 1-D velocity model in the northern Apennines shows a Moho depth of 35.0±1.2 km with low Pg velocity of 6.02 km/s. The strong low velocity anomalies in the lower crust beneath the Apennines have been reported in many previous tomographic studies [e.g. *Alessandrini et al.*, 1995; *Chiarabba and Amato*, 1996; *Di Stefano et al.*, 1999, 2006]. The low average Pg velocity beneath the northern Apennines can be explained by the low velocity anomalies in the lower crust. Also, the low velocity anomalies beneath the northern Apennines coincide with strong negative Bouguer anomalies in the area [*Di Stefano et al.*, 1999], suggesting some remarkable thermal effects active beneath the northern Apennines. To this regard, *Di Stefano et al.* [1999] interpreted the low-velocity and low-density anomalies as lower crust rocks heated by the uplifted asthenosphere in front of the Adriatic slab. This is consistent with the large attenuation of Pn phases observed by *Mele et al.* [1998] who also suggested the existence of a pronounced thermal anomaly at depth.

In the central Apennines, our results evidence a high Pg velocity of 6.34 km/s with the Moho depth of 33.2±1.6 km. *Di Stefano et al.* [1999] relate these high P-wave velocities to the limestone stack units composing the central-southern part of the Apennines. Our 1-D velocity model in the southern Apennines gives an average Pg velocity of 6.27 km/s with a Moho depth of 33.7±1.7 km, in agreement with previous tomographic results [*Alessandrini et al.*, 1995; *Chiarabba and Amato*, 1996].

Waveforms and travel-times from the 1-D velocity models obtained in this study fit the observed data generally well. However, there are still discrepancies between the synthetics and the observed data. These discrepancies can be caused by lateral velocity hetero-

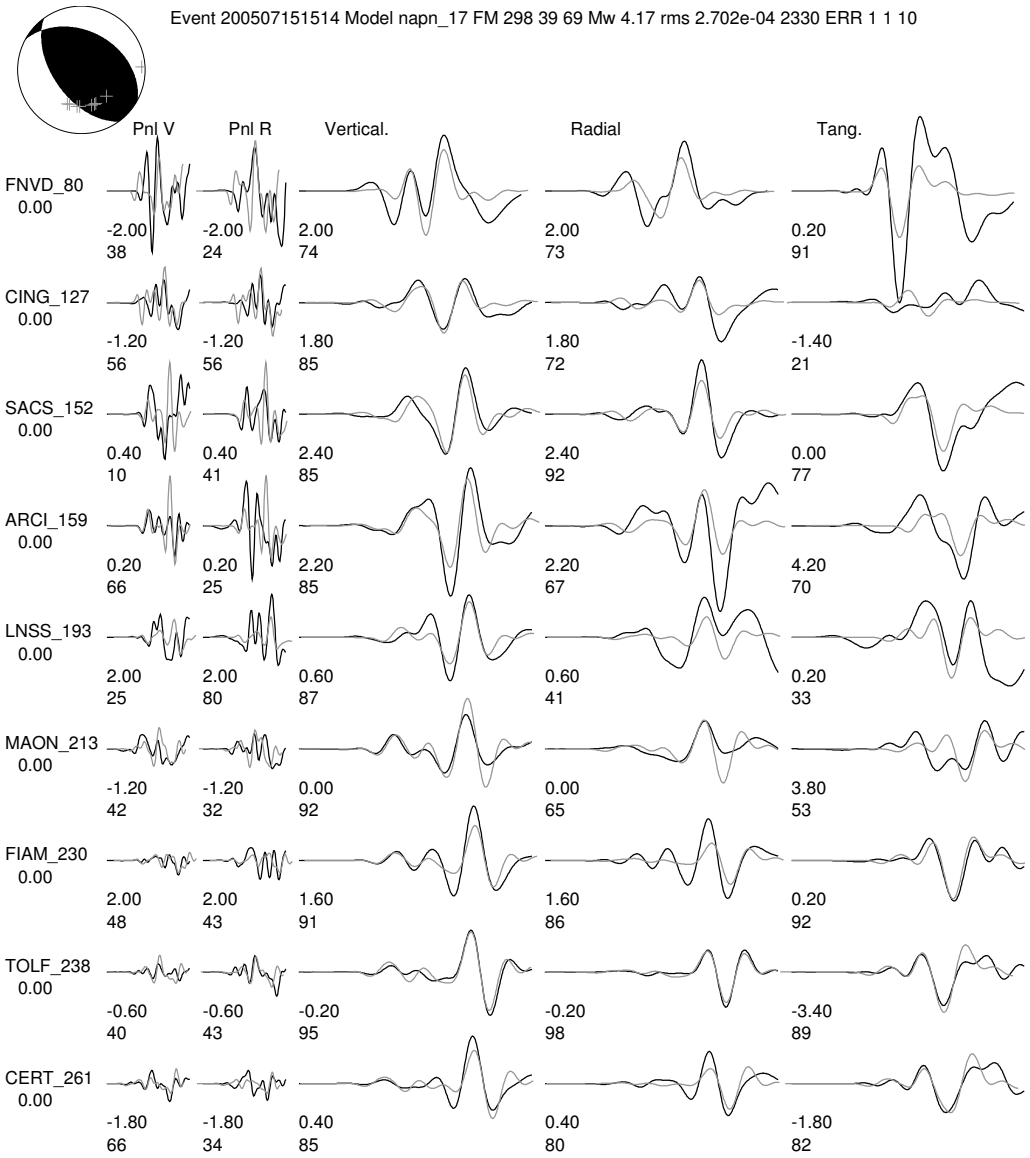

Figure 14. Waveform fits for event 200507151514. Data are indicated by black lines, synthetics are represented by gray lines. Station names plus epicentral distances are given on the left. The time shift in seconds and cross-correlation coefficients are shown below each waveform segment.

Table 1. Source Depths and Focal Mechanisms (FM) of 37 Earthquakes

Event ID	Origin Time and Location			Depth and FM		
	Date	o, GMT	Lon./Lat.	h, km	M_w	$\phi/\delta/\lambda$
200411250723	04/11/25	07:26:13.6	15.74/43.07	7.0	3.9	250/45/63
200411290105	04/11/29	01:08:10.8	15.36/43.07	9.0	3.7	292/36/78
200412040213	04/12/04	02:16:11.3	15.46/43.08	9.0	3.7	279/30/81
200412090241	04/12/09	02:44:25.3	13.79/42.79	15.0	4.0	350/12/100
200501311041	05/01/31	10:44:49.8	16.88/39.66	35.0	4.1	28/78/-180
200503131745	05/03/13	17:48:15.5	13.28/42.52	9.0	3.6	98/85/-170
200504120028	05/04/12	00:31:51.6	13.38/43.09	19.0	3.7	172/90/-12
200504181056	05/04/18	10:59:18.6	9.35/44.72	31.0	3.9	281/69/126
200504190739	05/04/19	07:42:01.2	9.72/44.77	25.0	4.2	261/65/12
200504190824	05/04/19	08:27:39.9	9.69/44.77	27.0	4.0	81/79/-140
200504231908	05/04/23	19:11:41.7	16.83/39.46	21.0	4.2	281/59/125
200504271305	05/04/27	13:08:08.6	12.73/43.24	5.0	3.5	109/42/-89
200504300807	05/04/30	08:10:25.1	9.32/44.69	13.0	3.7	1/84/-11
200505051318	05/05/05	13:21:21.9	13.71/41.89	15.0	3.7	108/78/-167
200505170029	05/05/17	00:32:13.6	10.19/43.62	19.0	3.7	217/70/10
200505211952	05/05/21	19:55:19.0	14.52/40.99	7.0	3.5	302/30/-6
200506020302	05/06/02	03:05:50.6	15.31/39.59	7.0	3.7	278/73/-172
200506050415	05/06/05	04:18:46.3	9.32/44.71	31.0	3.6	178/30/39
200507151514	05/07/15	15:17:18.0	12.11/44.21	17.0	4.1	298/39/69
200507211538	05/07/21	15:41:42.6	14.85/39.40	7.0	3.8	184/68/41
200509071237	05/09/07	12:40:33.4	16.32/38.71	21.0	3.9	164/78/-180
200509272230	05/09/27	22:33:09.3	17.10/38.62	29.0	3.9	38/79/141
200510301906	05/10/30	19:09:46.8	15.93/38.53	15.0	3.5	208/32/-139
200511082107	05/11/08	21:10:26.6	12.25/44.15	15.0	3.6	282/61/71
200511181832	05/11/18	18:35:22.6	17.21/39.12	27.0	3.9	121/33/-12
200512151325	05/12/15	13:28:39.6	12.76/42.74	9.0	4.0	257/43/-33
200604172139	06/04/17	21:42:55.7	10.28/43.37	9.0	3.7	77/90/-180
200609071528	06/09/07	15:31:43.7	16.16/40.58	27.0	4.3	11/62/-18
200610200008	06/10/20	00:11:58.8	10.36/45.71	15.0	4.0	28/79/-174
*200411242256	04/11/24	22:59.38.0	10.83/45.54	17.0	4.9	342/81/56
*200411250618	04/11/25	06:21:18.7	15.16/43.13	7.0	5.0	279/28/69
*200412030810	04/12/03	08:13:12.8	15.12/42.99	9.0	4.5	260/58/37
*200508221159	05/08/22	12:02:06.0	12.49/41.61	9.0	4.6	162/85/180
*200604162111	06/04/16	21:14:57.2	11.92/44.09	25.0	4.5	288/33/84
*200604170241	06/04/17	02:44:10.7	17.38/39.54	27.0	4.7	239/84/-159
*200605290217	06/05/29	02:20:02.9	15.90/41.73	29.0	4.5	272/42/117
*200606221931	06/06/22	19:34:54.3	16.67/39.75	35.0	4.8	110/70/16

* Source depths and focal mechanisms are also determined by MedNet using the surface wave RCMT method, and the comparison of source mechanisms from our study with MedNet solutions for them are shown in Fig. 15.

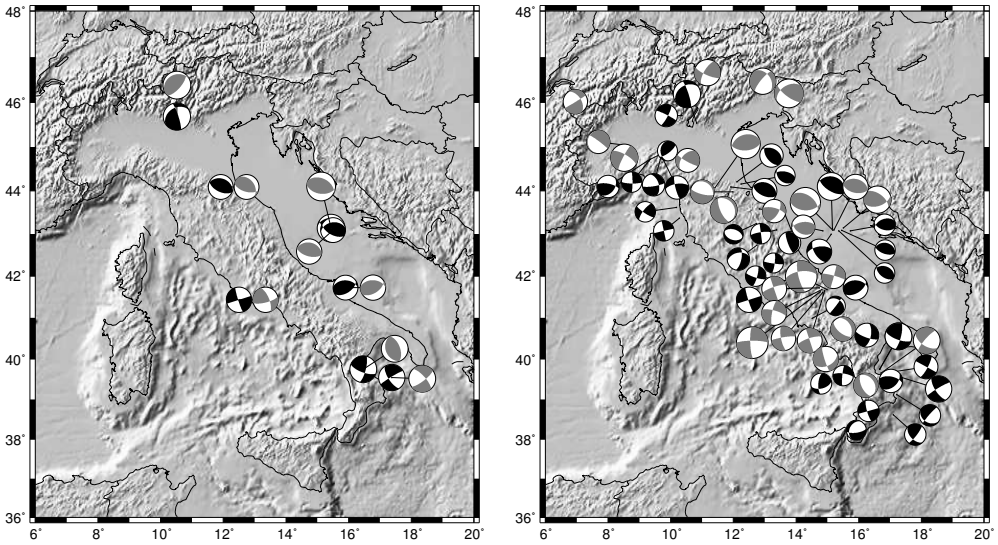

Figure 15. Left: comparison of source mechanisms from this study (black) with MedNet solutions (gray) for 8 events with $Mw > 4.0$. Right: the lower-hemisphere projections of focal mechanisms of 37 events determined in this study (black), and 26 MedNet solutions (gray) for the $Mw > 4.0$ since 2001.

geneities un-accounted by the one-dimensional velocity model. This is supported by the relevant lateral variations observable in the P-wave tomography (Fig. 5).

The results from the source mechanism inversion also show time shifts up to ±8 s between observed surface waves and synthetics (Fig. 16). The time shifts indicate local variations of the velocity structure. Since our 1-D best velocity models are derived from averaging all the paths in each subregion, it is possible that at some stations synthetics arrive earlier or later than observations. In the northern and central Apennines, the shift values are small, implying that our velocity models are probably good approximations for those regions. In the southern Apennines, the shift amounts are large and show both positive and negative values owing to the inclusion of different tectonic units within the same region (Fig. 5). Also, we observe that the velocities of the resolved model beneath the Adriatic Sea are too fast (Fig. 16). To this regard, we note that combination of this map of the anomalies together with the regionalized velocity models can be used to predict time shifts while determining source parameters of future earthquakes [*Tan et al.*, 2006].

Source mechanisms determined from the regionalized velocity models show that a compressional regime dominates the Adriatic sea and the outer margin of the northern Apennines, and an extensional regime characterizes most of the Apenninic belt. In the general context of the N-S convergence of Europe and Africa, the contemporaneous existence of differently oriented tectonic units in such a small volume has been widely discussed [e.g. *Westaway*, 1990; *Jolivet and Faccenna*, 2000; *Gvirtzman and Nur*, 2001; *Margheriti et al.*, 2003]. It is thought that the collision between the African and Eurasian plates led to both a wide belt of crustal deformation and a fragmentation of the lithosphere into a number of microplates trapped between the large plates [*Margheriti et al.*, 2003]. The complex interactions among these microplates resulted in a jigsaw-puzzle-like tectonic pattern. The compressional regime beneath the Adriatic sea is consistent with the N-S compressional tectonics, and it is probably related to the relative motion of the Adriatic microplate which moves coherently with Africa. The extensional regime beneath the Apennines belt agrees with the regional NE-trending extension, and may reflect the slab retreat such as the prolonged retreat of the Adriatic-Ionian slab [*Montone et al.*, 1999].

In summary, with regional travel-time and waveform data, we derive 1-D regionalized velocity models for four subregions by applying the GA inversion. Our 1-D models generally result in improved waveform fits between observed data and synthetics. We think that these results can be applicable to real-time seismic monitoring, extended fault studies, and for the generation of shakemaps. With the 1-D regionalized models we determine

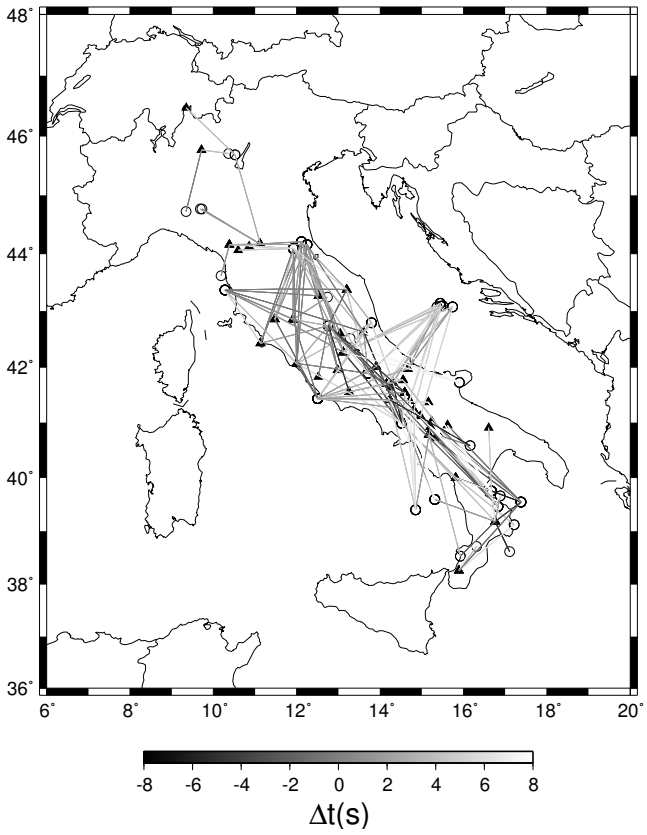

Figure 16. Surface wave time shifts from the CAP inversion (positive shift means that the observation is later than predicted by the model).

source depths and focal mechanisms for 37 events with magnitude larger than 3.5 by waveform inversion. Our results show that normal and strike-slip faulting source mechanisms with NE extension dominate the Apenninic belt, thrust faulting events mostly occurred in the Adriatic sea and the outer margin of the northern Apennines.

Acknowledgments. We are grateful to Raffaele Di Stefano for offering the travel-time tomography data, Lucia Margheriti and Giuliana Mele for providing tectonic data. We thank Claudio Chiarabba, Laura Scognamiglio and Elisa Tinti for their helpful comments and discussions. We also thank David L. Carroll for offering the GA code. We are thankful to J. Hardebeck and two anonymous reviewers for their comments and suggestions to improve the manuscript. This work was carried out in the framework of the DPC-S4 project.

References

Amato, A., B. Alessandrini, and G. B. Cimini (1993), Teleseismic wave tomography of Italy, in *Seismic Tomography: Theory and Practice*, pp. 361–396, eds Iyer, H. M., H. Hirahara, Chapman and Hall, London.

Amato, A., L. Margheriti, R. Azzara, A. Basili, C. Chiarabba, M. G. Ciaccio, G. B. Cimini, M. Di Bona, A. Frepoli, F. P. Lucente, C. Nostro, and G. Selvaggi (1998), Passive seismology and deep structure in central Italy, *Pure Appl. Geophys.* **151**, 479–493.

Alessandrini, B., L. Beranzoli, and F. M. Mele (1995), 3-D crustal P-wave velocity tomography of the Italian region using local and regional seismicity data, *Ann. Geofis.* **38**, 189–211.

Barchi, M. R., G. Minelli, and G. Pialli (1998), The CROP 03 profile: a synthesis of results on deep structures of the northern Apennines, *Mem. Soc. Geol. Ital.* **52**, 383–400.

Bhattacharyya, J., A. F. Sheehan, K. Tiampo, and J. Rundle (1999), Using a genetic algorithm to model broadband regional waveforms for crustal structure in the western United States, *Bull. Seism. Soc. Am.* **89**, 202–214.

Billings, S., B. Kennett, and M. Sambridge (1994), Hypocenter location: genetic algorithms incorporating problem specific information, *Geophys. J. Int.* **118**, 693–706.

Chang, S.-J., C.-E. Baag, and C. A. Langston (2004), Joint analysis of teleseismic receiver functions and

surface wave dispersion using the genetic algorithm, *Bull. Seism. Soc. Am.* **94**, 691–704.

Chang, S.-J., and C.-E. Baag (2006), crustal structure in Southern Korea from joint analysis of regional broadband waveforms and travel times, *Bull. Seism. Soc. Am.* **96**, 856–870.

Chiarabba, C., and A. Amato (1996), Crustal velocity structure of the Apennines (Italy) from P-wave travel time tomography, *Ann. Geofis.* **39**, 1133–1148.

Chiarabba, C., and A. Frepoli (1997), Minimum 1D velocity models in central and southern Italy: a contribution to better constrain hypocentral determinations, *Ann. Geofis.* **40**, 937–954.

Chiarabba, C., L. Jovane, and R. DiStefano (2005), A new view of Italian seismicity using 20 years of instrumental recordings, *Tectonophysics* **395**, 251–268.

Dewey, J. F., M. L. Helman, E. Turco, D. W. H. Hutton, and S. P. Knott (1989), Kinematics of the western Mediterranean, in *Alpine Tectonics*, eds Coward, M. P., D. Dietrich, and R. G. Park, *Geol. Soc. Lond. Spec. Publ.* **45**, 265–283.

Di Stefano, R., C. Chiarabba, F. Lucente, and A. Amato (1999), Crustal and uppermost mantle structure in Italy from the inversion of P-wave arrival times: geodynamic implications, *Geophys. J. Int.* **139**, 483–498.

Di Stefano, R., E. Kissling, C. Chiarabba, A. Amato, and D. Giardini (2006), Shallow subduction beneath Italy: three-dimensional images of the Adriatic-European-Tyrrhenian lithosphere system with automatically detected high quality P-wave arrival times, *submitted to J. Geophys. Res.*, 2006.

Dreger, D. S., and D. V. Helmberger (1990), Broadband modeling of local earthquakes, *Bull. Seism. Soc. Am.* **80**, 1162–1179.

Dreger, D. S., and D. V. Helmberger (1993), Determination of source parameters at regional distances with single station or sparse network data, *J. Geophys. Res.* **98**, 8107–8125.

Du, Z. J., and G. F.Panza (1999), Amplitude and phase differentiation of synthetic seismograms: a must for waveform inversion at regional scale, *Geophys. J. Int.* **136**, 83–98.

Ekström, G., A. Morelli, E. Boschi, A. M. Dziewonski (1998), Moment tensor analysis of the central Italy earthquake sequence of September-October 1997, *Geophys. Res. Lett.* **25**, 1971–1974.

Goldberg, D. E. (1989), *Genetic Algorithm in Search Optimization and Machine Learning*, Addison-Wesley, MA.

Gualtieri, L., and R. Cassinis (1998), The deep structure of the Northern Apennines imaged by ray tracing depth migration of Near Vertical seismic data, *Mem. Soc. Geol. Ital.* **52**, 163–173.

Gualtieri, L., R. De Franco, and A. Mazzotti (1998), A velocity model along the CROP 03 profile derived from expanding spread experiments, *Mem. Soc. Geol. Ital.* **52**, 139–152.

Gvirtzman, Z. and A. Nur (2001), Residual topography, lithospheric structure and sunken slabs in the central Mediterranean, *Earth Planet. Sci. Lett.* **187**, 117–130.

Hirn, A., and M. Sapin (1997), Crustal structure beneath Corsica, *Boll. Geofis. Teor. Appl.* **75–76**, 233–235.

Holland, J. H. (1975), *Adaptation in Natural and Artificial System: An Introduction with Application to Biology, Control and Artificial Intelligence*, University of Michigan Press, Ann Arbor, MI.

Improta, L., G. Iannacone, P. Capuano, A. Zollo, and P. Scandone (2000), Inferences on the upper crustal structure of Southern Appennines (Italy) from seismic refraction investigations and subsurface data, *Tectonophysics* **317**, 273–297.

Jolivet, L., and C. Faccenna (2000), Mediterranean extension and the African-Eurasia collision, *Tectonics* **19**, 1095–1107.

Kennett, B. L. N., and M. S. Sambridge (1992), Earthquake location–genetic algorithms for teleseisms, *Phys. Earth Planet. Inter.* **75**, 103–110.

Kim, W., I.-K. Hahm, S. J. Ahn, and D. H. Lim (2006), Determining hypocentral parameters for local earthquakes in 1-D using a genetic algorithm, *Geophys. J. Int.* **166**, 590–600.

Kobayashi, R., and I. Nakanishi (1994), Application of genetic algorithms to focal mechanism determination, *Geophys. Res. Lett.* **21**, 590–600.

Kummerow, J., R. Kind, O. Oncken, P. Giese, T. Ryberg, K. Wylegalla, F. Scherbaum, and TRANSALP Working Group (2004), A natural and controlled source seismic profile through the Eastern Alps: TRANSALP, *Earth Planet. Sci. Lett.* **225**, 115–129

Louis, S. J., Q. Chen, and S. Pullammanappallil, Seismic velocity inversion with genetic algorithms, *CEC99, 1999 Congress on Evolutionary Computation*, Mayflower Hotel, Washington D.C., 855–861.

Malinverno, A., and W. B. F. Ryan (1986), Extension in the Tyrrhenian Sea and shortening in the Apennines as a result of arc migration driven by sinking of the lithosphere, *Tectonics* **5**, 227–245.

Margheriti, L., F. P. Lucente, and S. Pondrelli (2003), SKS splitting measurements in the Apenninic-Tyrrhenian domain Italy and their relation with lithospheric subduction and mantl convection, *J. Geophys. Res.* **108**(B4), 2218, doi: 10.1029/2002JB001793.

Mele, G., A. Rovelli, D. Seber, T. Hearn, and M. Barazangi (1998), Compressional velocity structure and anisotropy in the uppermost mantle beneath Italy and the surrounding regions, *J. Geophys. Res.* **103**(B6), 12,529–12,543.

Mele, G., and E. Sandvol (2003), Deep crustal roots beneath the northern Apennines inferred from teleseismic receiver functions, *Earth Planet. Sci. Lett.* **211**, 69–78.

Montone, P., A. Amato, and S. Pondrelli (1999), Active stress map of Italy, *J. Geophys. Res.* **104**, 25,595–25,610.

Moya, A., J. Aguirre, and K. Irikura (2000), Inversion of source parameters and site effects from strong ground motion records using genetic algorithms, *Bull. Seism. Soc. Am.* **90**, 977–992.

Patacca, E., and P. Scandone (1989), The role of the passive sinking of a relic lithospheric slab, in *The Lithosphere in Italy*, pp. 157–176, eds Boriani, A., M. Bonafede, P. G. Piccardo, and G. B. Vai, Academia Nazionale dei Lincei, Rome.

Patacca, E., R. Sartori, and P. Scandone (1990), Tyrrhenian Basin and Apenninic Arcs: kinematic relations since Late Tortonian times, *Mem. Soc. Geol. Ital.* **45**, 425–451.

Paul, A., M. Cattaneo, F. Thouvenot, D. Spallarossa, N. Béthoux, and J. Fréchet (2001), A three-dimensional crustal velocity model of the southerwestern Alps from local earthquake tomography, *J. Geophys. Res.* **106**(B9), 19,367–19,389.

Piromallo, C., and A. Morelli (1997), Imaging the Mediterranean upper mantle by *P*-wave travel time tomography, *Ann. Geofis.* **40**, 963–979.

Piromallo, C., and A. Morelli (2003), *P*-wave tomography of the mantle under the Alpine-Mediterranean area, *J. Geophys. Res.* **108**(B2), 757, doi:10.1029/2002JB001.

Pondrelli, S., S. Salimbeni, G. Ekström, A. Morelli, P. Gasperini and G. Vannucci (2006), The Italian CMT dataset from 1977 to the present, *Phys. Earth Planet. Inter.* **159**, 286-303, doi: 10.1016/j.pepi.2006.07.008.

Pontevivo, A., and G. Panza (2002), Group velocity tomography and regionalization in Italy and bordering areas, *Phys. Earth Planet. Inter.* **134**, 1–15.

Ponziani, F., R. De Franco, G. Minelli, G. Biella, C. Federico, and G. Pialli (1995), Crustal shortening and duplication of the Moho in the Northern Apennines: view from seismic refraction data, *Tectonophysics* **252**, 391–419.

Rodgers, A. J., and S. Y. Schwartz (1998), Lithospheric structure of the Qiangtang Terrane, northern Tibetan Plateau, from complete regional waveform modeling: evidence for partial melt, *J. Geophys. Res.* **103**, 7137–7152.

Scarascia, S., A. Lozej, and R. Cassinis (1994), Crustal structures of the Ligurian, Tyrrhenian and Ionian seas and adjacent onshore areas interpreted from wide-angle seismic profiles, *Boll. Geofis. Teor. Appl.* **36**, 5–19.

Scarascia, S., and R. Cassinis (1997), Crustal structures in the central-eastern Alpine sector: A revision of the available DSS data, *Tectonophysics* **271**, 157–188.

Scognamiglio, L., E. Tinti, and A. Michelini (in preparation), Real-time regional moment tensor estimation using the Italian broadband network, in preparation.

Selvaggi, G., and C. Chiarabba (1995), Seismicity and *P*-wave velocity image of the southern Tyrrhenian subduction zone, *Geophys. J. Int.* **121**, 818–826.

Song, X. J., D. V. Helmberger, and L. Zhao (1996), Broadband modeling of regional seismograms: The Basin and Range crustal structure, *Geophys. J. Int.* **125**, 15–29.

Spakman, W., S. van der Lee, and R. van der Hilst (1993), Travel-time tomography of the European-Mediterranean mantle down to 1400 km, *Phys. Earth Planet Inter.* **79**, 3–74.

Tan, Y., L. Zhu, D. V. Helmberger, and C. K. Saikia (2006), Locating and modeling regional earthquakes with two stations, *J. Geophys. J. Res.* **111**, B01306, doi:10.1029/2005JB003775.

Waldhauseret, F., E. Kissling, J. Ansorge, and S. Mueller (1998), Three-dimensional interface modeling with two-dimensional seismic data: the Alpine crust-mantle boundary, *Geophys. J. Int.* **135**, 264–278.

Waldhauseret, F., R. Lippotsch, E. Kissling, and J. Ansorge (2002), High-resolution teleseismic tomography of upper-mantle structure using an a priori three-dimensional crustal model, *Geophys. J. Int.* **150**, 403–414.

Westaway, R. (1990), Present-day kinematics of the plate boundary zone between African and Europe, from the Azores to the Aegean, *Earth Planet. Sci. Lett.* **96**, 393–406.

Westaway, R. (1992), Seismic moment summation for historical earthquakes in Italy: tectonic implications, *J. Geophys. Res.* **97**, 15,437–15,464.

Zeng Y., and J. G. Anderson (1996), a composite source model of the 1994 Northridge earthquake using genetic algorithm, *Bull. Seism. Soc. Am.* **86**, S71–S83.

Zhao, L. S., and D. V. Helmberger (1994), Source estimation from broadband regional seismograms, *Bull. Seism. Soc. Am.* **84**, 91–104.

Zhou, R., F. Tajima, and P. L. Stoffa (1995), Application of genetic algorithms to constrain near-source velocity structure for the 1989 Sichuan earthquakes, *Bull. Seism. Soc. Am.* **85**, 590–605.

Zhu, L., and D. V. Helmberger (1996), Advancement in source estimation techniques using broadband regional seismograms, *Bull. Seism. Soc. Am.* **86**, 1634–1641.

Zhu, L., and L. A. Rivera (2002), A note on the dynamic and static displacements from a point source in multi-layered media, *Geophys. J. Int.* **148**, 619–627.

Zhu, L., Y. Tan, D. V. Helmberger, and C. K. Saikia (2006), Calibration of the Tibetan Plateau using regional seismic waveforms, *Pure Appl. Geophys.* **163**, 1193–6213.

This preprint was prepared with AGU's LaTeX macros v5.01, with the extension package 'AGU^{++}' by P. W. Daly, version 1.6b from 1999/08/19.